POLITECNICO DI TORINO
Repository ISTITUZIONALE

Synthesis and characterization of new nano organic-inorganic hybrid (TBA)4PW11Fe@TiO2@PVA as a promising phase-transfer catalyst for oxidative desulfurization of

Original
Synthesis and characterization of new nano organic-inorganic hybrid (TBA)4PW11Fe@TiO2@PVA as a promising phase-transfer catalyst for oxidative desulfurization of real fuel / Ali Rezvani, M., Noori Oghoulbeyk, Z., Khandan, S., Mazzei, H.. - In: POLYHEDRON. - ISSN 0277-5387. - ELETTRONICO. - 177:(2020), p. 114291. [10.1016/j.poly.2019.114291]

Availability:
This version is available at: 11583/2965636 since: 2022-06-01T19:11:09Z

Publisher:
Elsevier Ltd

Published
DOI:10.1016/j.poly.2019.114291

Terms of use:

This article is made available under terms and conditions as specified in the corresponding bibliographic description in the repository

Publisher copyright
Elsevier postprint/Author's Accepted Manuscript

© 2020. This manuscript version is made available under the CC-BY-NC-ND 4.0 license http://creativecommons.org/licenses/by-nc-nd/4.0/.The final authenticated version is available online at: http://dx.doi.org/10.1016/j.poly.2019.114291

(Article begins on next page)

26 November 2026

Synthesis and characterization of $(TBA)_4PW_{11}Fe@TiO_2@PVA$ nanocomposite as a promising phase-transfer catalyst for oxidative desulfurization of gas oil

Mohammad Ali Rezvani [a]*, Zahra Noori Oghoulbeyk [a], Sahar Khandan [a], Hernan Gabriel Mazzei [b]

[a] Department of Chemistry, Faculty of Science, University of Zanjan, 451561319, Zanjan, Iran

[b] Instituto de Ciencia y Tecnología de los Alimentos (ICTA–FCEFyN–UNC), Físicas y Naturales, Facultad de Ciencias Exactas, Universidad Nacional de Córdoba, Av. Vélez Sarsfield 1611, X5016GCA, Córdoba, Argentina

*Corresponding author: E-mail: marezvani@znu.ac.ir ; Tel./Fax: +98 (24) 3305 2477

Graphical Abstract

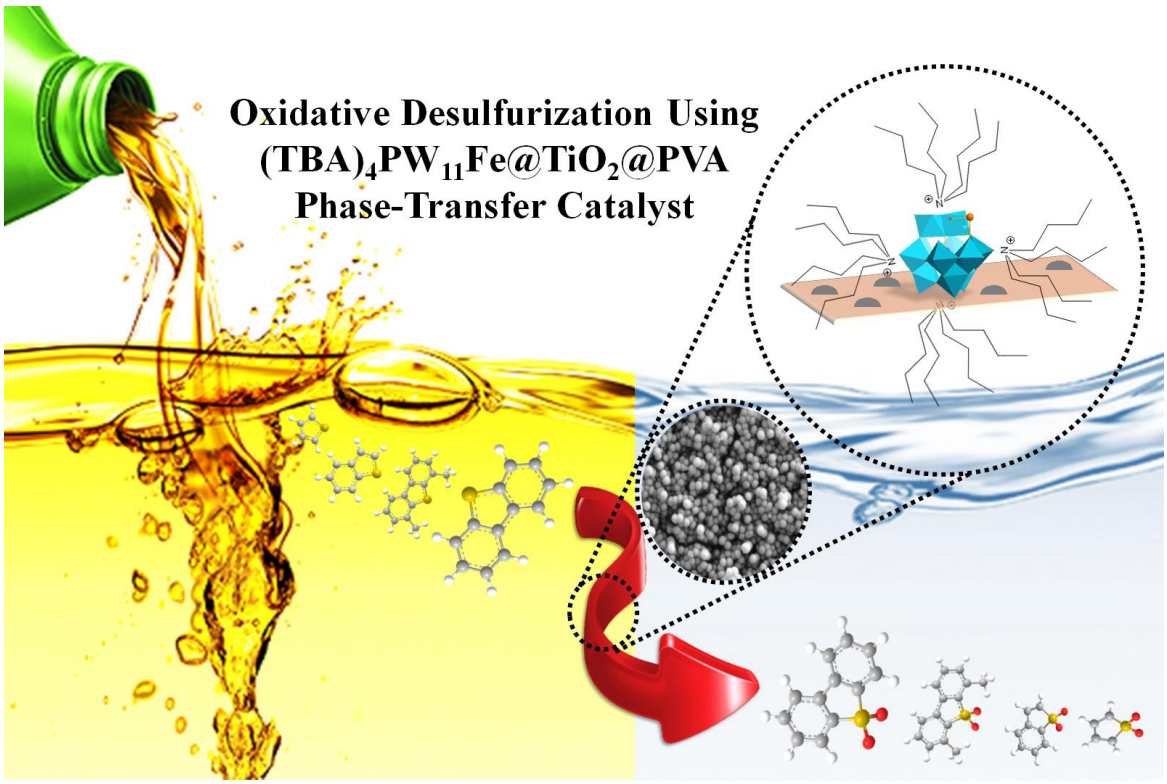

Abstract

Nowadays, the development of a new and sustainable desulfurization strategy to achieve deep removal of organic sulfur compounds from fuels is necessary. In this work, an efficient oxidative desulfurization (ODS) process of real gas oil and model oils was introduced using $(TBA)_4PW_{11}Fe@TiO_2@PVA$ phase-transfer catalyst. The catalyst was successfully prepared by the composition of the quaternary ammonium salt of mono iron-substituted phosphotungstate (abbreviated as $(TBA)_4PW_{11}Fe$), titanium dioxide (TiO_2), and polyvinyl alcohol (PVA). The nanocomposite obtained was characterized through FT-IR, UV-vis, XRD, and SEM techniques. The spectroscopic characterization revealed that the $(TBA)_4PW_{11}Fe$ was immobilized on the surface of TiO_2@PVA. Also, the results of catalytic tests showed the outstanding ODS performance of $(TBA)_4PW_{11}Fe@TiO_2@PVA$ in the removal of thiophenic compounds. Under optimized reaction conditions, the ODS efficiencies of benzothiophene (BT), dibenzothiophene (DBT), 4-methyldibenzothiophene (4-MDBT), and 4,6-dimethyldibenzothiophene (4,6-DMDBT) reach 96, 99, 97, and 98%, respectively. The desulfurization system can be recycled five times with merely a slight decrease in activity.

Keywords: Heteropolyoxometalate, Nanocomposite, Phase-transfer catalyst, Oxidative desulfurization

1. Introduction

Petroleum and its derivatives are mainly composed of a mixture of hydrocarbons with variable amounts of sulfur-, nitrogen-, and oxygen-containing substances. Sulfur compounds, either organic or inorganic, are known to be harmful to oil refinery products such as gas oil and gasoline [1-3]. The combustion of transportation fuels with a high level of sulfur liberates sulfur oxides (SO_x), which are corrosive gases [4]. Since the adverse effects of SO_x comprise from the acid rain to serious health issues, the stringent standards for sulfur content in fuel have

undergone in many countries [5]. For instance, the European Union (E.U.) legislation and the U.S. Environmental Protection Agency (EPA) set the standards to ultra-low sulfur levels (<10 ppm) [6]. To meet SO_x pollution control standards, many efforts have been taken towards the investigation of more effective and economical desulfurization techniques [7-11]. Hydro-desulfurization (HDS) is the most used common method by refineries during the past several decades [12]. According to HDS process, the organic sulfur molecules are converted to hydrogen sulfides in the presence of hydrogen gas under high-pressure (10-130 atm) and high-temperature (300-400 °C) [13]. Due to its high cost and low efficiency in treating thiophenic compounds, the alternative non-HDS approaches have been studied. An array of methods, including extraction [14], adsorption [15], oxidation [16] etc. Among them, oxidative desulfurization (ODS) is considered as a well-established complementary desulfurization process [17]. With ODS, a very low level of sulfur can be achieved by two steps at the same time or sequentially; oxidation of sulfur-containing compounds into sulfones and sulfoxides with an oxidant, followed by *in situ* extraction of products using an extraction solvent [18]. The oxidation reactions using hydrogen peroxide (H_2O_2) as a common oxidant usually involves two or three phases, which inhibits the rate of desulfurization [19,20]. For overcoming this obstacle, the oxygen-containing chemicals can be produced through the composition of H_2O_2 with organic acids and/or the application of appropriate catalysts [21,22].

Catalysis by heteropolyoxometalates (HPOMs) and their related compounds is a field of growing importance over the past decade [23-25]. Particularly, the Keggin-type HPOMs with the general formula of $[XM_{12}O_{40}]^{n-}$ (X = P or Si and M = Mo or W) have been extensively studied as oxidation catalysts due to their impressive redox properties, thermal stability, super acidity, and intrinsic resistance to oxidative decomposition [26-28]. As a counterpart, it is known that the general drawback of bulk HPOMs is their high solubility in aqueous mediums, which make the active sites inaccessible for water/oil biphasic reactions [29]. To confront this

limitation, the quaternary ammonium salts have been used as a countercation to synthesize HPOM-based phase-transfer catalysts [30,31]. Moreover, several studies have been shown that immobilization of HPOMs on support materials such as metal oxides and polymers can provide their catalytic activity in ODS process [32,33]. In recent years, metal oxide@polymer composites have been widely used for catalysis thanks to their outstanding properties of processibility and low-cost [34,35]. Among the different polymers, polyvinyl alcohol (PVA) revealed to be very attractive to immobilize metal oxides from HPOM clusters to TiO_2 particles [36,37]. Interestingly, the strong interaction between hydroxyl groups of PVA and oxygen groups of metal oxides can accelerate the electron transfer, causing high redox activity in oxidation reactions [22,36]. Further, the improvement in both catalytic performance and chemical stability of PVA can be done by modifying its surface with semiconductor metal oxides. In this regard, TiO_2 can be an attractive candidate because of its abundance, good chemical stability, non-toxicity, and high catalytic activity [38].

Herein, for the first time, we report the fabrication of $(TBA)_4PW_{11}Fe@TiO_2@PVA$ nanocomposite as the phase-transfer catalyst. Characterization studies were done by techniques such as FT-IR, UV-vis, XRD, and SEM. Then, the prepared catalyst has been applied to remove sulfur-containing molecules from real gas oil and model oils through the ODS process. The experimental results indicated that $(TBA)_4PW_{11}Fe@TiO_2@PVA$ composite exhibited obvious catalytic activity toward the reduction of sulfur concentration using hydrogen peroxide/acetic acid (H_2O_2/HOAc) oxidant. Special importance was addressed on the efficient catalytic performance of $(TBA)_4PW_{11}Fe@TiO_2@PVA$ phase-transfer catalyst to achieve deep ODS treatment.

2. Experimental section

2.1. Materials

The following chemicals and reagents were used as received without further purification: sodium tungstate dihydrate ($Na_2WO_4 \cdot 2H_2O$), disodium hydrogen phosphate (Na_2HPO_4), Iron (III) nitrate nonahydrate ($Fe(NO_3)_3 \cdot 9H_2O$), tetra (*n*-butyl) ammonium bromide (TBAB), polyvinyl alcohol (PVA), titanium dioxide (TiO_2), benzothiophene (BT, 97%), dibenzothiophene (DBT, 98%), 4-methyldibenzothiophene (4-MDBT, 97%), 4,6-dimethyldibenzothiophene (4,6-DMDBT, 97%), *n*-heptane, hydrogen peroxide (H_2O_2, 30 vol.%), glacial acetic acid (HOAc), and acetonitrile (MeCN) were supplied by Sigma-Aldrich.

2.2. Synthesis of $(TBA)_4PW_{11}Fe$

The quaternary ammonium salt of mono iron-substituted phosphotungstate, $(TBA)_4PW_{11}Fe$, was synthesized according to the literature [27]. The required amount of $Na_2WO_4 \cdot 2H_2O$ (3.29 g) was dissolved in 20 mL of distilled water under magnetic stirring. Then, Na_2HPO_4 (0.13 g) and $Fe(NO_3)_3 \cdot 9H_2O$ (0.49 g) were immersed in the above aqueous solution. The pH was adjusted to 4.5 and the resulting mixture was heated to 80 °C. After completing the reaction, TBAB (1.45 g) was dissolved in 5 mL of distilled water and immediately added to the mixture to form a milky white precipitate. The final product was separated by filtration, washed with ether, and air dried.

2.3. Synthesis of $(TBA)_4PW_{11}Fe@TiO_2$@PVA nanocomposite

The nanocomposite was prepared by *in situ* composition of $(TBA)_4PW_{11}Fe$, TiO_2, and PVA through the sol-gel method. In a typical synthesis process, the powder of TiO_2 (0.05 g) was added to a solution of PVA (0.10 g) in 50 mL of hot distilled water under stirring condition. Then, the amounts of $(TBA)_4PW_{11}Fe$ (0.10 g) were added to the mixture and stirred at 60 °C for 2 h. After heating and achieving a complete dispersion of metal oxide powders in PVA, the sol was converted into a clear gel. Finally, the gel was cast on a clean glass plate and dried at 80 °C for 2 h to form $(TBA)_4PW_{11}Fe@TiO_2$@PVA nanocomposite.

2.4. Characterization methods

Powder X-ray diffraction (XRD) patterns of reactants and products were obtained on a Bruker D8 Advance X-ray diffractometer with monochromatic Cu (Kα) radiation, using voltage of 40 kV and current of 30 mA. The morphological properties of the samples were determined by scanning electron microscopy (SEM) on LEO 1455 VP. The chemical groups and chemical composition of materials were identified by the Fourier transform infrared (FT-IR) spectra. The samples were prepared by KBr pellet method and the data were recorded using a Thermo-Nicolet-iS10 instrument. Ultraviolet-visible (UV-vis) spectra were recorded on a double beam Analytical Jena-Specord 205 spectrometer in the region 190-400 nm. The content of total sulfur in model oils and real gas oil were determined by X-ray fluorescence (XRF) with a TANAKA X-ray fluorescence spectrometer RX-360 SH.

2.5. ODS process of model oils and real gas oil

A typical ODS procedure of model oil was carried out according to the following steps: 50 mL of *n*-heptane containing thiophenic compound (BT, DBT, 4-MDBT, and 4,6-DMDBT) with an initial concentration of 500 ppm was added into a 100 mL two-necked flask. The flask was placed in an oil bath coupled with a thermometer and magnetic stirrer. The model oil was heated to 30, 40, 50, and 60 °C in the separate runs and the temperature was kept constant during the reaction. Subsequently, the amount of $(TBA)_4PW_{11}Fe@TiO_2@PVA$ phase-transfer catalyst and 6 mL of H_2O_2/HOAc oxidant (in v/v ratio of 1:1) were added to the fuel within 30 min. After it has been stirred vigorously for 2 h, the mixture was cooled to room temperature, followed by addition of 10 mL of MeCN as an extraction solvent. The treated fuel was settled for 10 min to obtain phase splitting. The upper oil phase was separated and the residual sulfur content was obtained through XRF method.

The ODS experiment of real gas oil was processed in the same manner as it was described above. In a typical test under optimized condition, 50 mL of gas oil (containing 9848 ppm of

sulfur) was added to the flask and heated to 60 °C. The $(TBA)_4PW_{11}Fe@TiO_2@PVA$ catalyst (0.10 g) and H_2O_2/HOAc oxidant (6 mL) were poured into the reaction vessel. The mixture was stirred magnetically at the predefined temperature for 2 h. After that, 10 mL of MeCN was utilized to extract the reaction products. When the ODS run was finished, the treated gas oil was separated from the aqua phase and analyzed by XRF based on D-4294 and D-3227 ASTM standards. The main specifications of gas oil before and after the desulfurization process are summarized in Table 1. The overall removal efficiency (X, %) of sulfur compounds from simulated fuels and actual gas oil in each ODS test was estimated using Eq. 1.

$$X(\%) = \left[1 - \frac{S_t}{S_i}\right] \times 100 \quad (1)$$

where S_i is the initial sulfur concentration in fuel, and S_f is the remaining sulfur concentration after ODS at time t, respectively.

For evaluating the regeneration performance of the catalyst, the $(TBA)_4PW_{11}Fe@TiO_2@PVA$ nanocomposite was separated from the reaction medium by filtration at the end of the ODS treatment. Whereafter, it was thoroughly washed several times with the dichloromethane to remove adsorbed residual products from the surface of the catalyst. The recovered sample was dried at 75 °C for 2 h and reused in the consequent desulfurization reaction under the conditions mentioned using the fresh fuel, oxidant, and extraction solvent.

(Table 1)

3. Results and discussion

3.1. Characterization of materials

FT-IR analysis was carried out to verify the successful preparation of $(TBA)_4PW_{11}Fe@TiO_2@PVA$ nanocomposite. As shown in Fig. 1(a), the absorption bands for the pure PVA at 884 and 1435 cm^{-1} are assigned to the stretching and bending vibrations of H–

C–H, respectively. At the same time, the peaks at 1096 and 1733 cm^{-1} corresponds to the stretching vibration modes of C–O–C and C=O in acetyl and vinyl acetate groups of PVA, respectively. The bands at 2875 and 2905 cm^{-1} indicate the asymmetric stretching vibration of CH_2 and CH_3 groups [36]. Moreover, strong broadband appeared at 3512 cm^{-1} which has been attributed to the stretching vibrations of the O–H groups. In Fig. 1(b) the absorption peaks in the range of 473-717 cm^{-1} are assigned to Ti–O bond of TiO_2 [39]. From the spectra of Keggin-type HPOM, the asymmetric stretching vibration bands of the $[PW_{11}Fe(H_2O)O_{39}]^{4-}$ anion can be observed at 793, 887, 962, and 1068 cm^{-1}, corresponding to the edge-sharing ($W–O_c–W$), corner-sharing ($W–O_b–W$), terminal ($W=O_d$), and the central ($P–O_a$) oxygen, respectively (Fig. 1(c)) [27]. Notably, the splitting of the P–O band into two branches (~1068 and 1070 cm^{-1}) clearly indicates that Fe transition metal ion was confidently introduced into the octahedral lacuna [36,40]. Further, the peaks at 1383 and 1483 cm^{-1} are assigned to the scissoring vibrations of C–H in the TBA cation [30]. Fig. 1(d) clearly shows the characteristic bands of $(TBA)_4PW_{11}Fe$ at 815, 960, and 1078 cm^{-1}. It provides that HPOM clusters retained its structure after immobilization on support materials. The evidence of the formation of intermolecular hydrogen bonding between the hydroxyl functional groups of PVA and the oxygens of $(TBA)_4PW_{11}Fe$ and TiO_2 can be obtained from some shifts in the spectrum of the catalyst compared to the bulk samples [27,41,42].

(Fig. 1)

Fig. 2 presents the UV-vis absorption spectra of TiO_2, $(TBA)_4PW_{11}Fe$, and $(TBA)_4PW_{11}Fe@TiO_2@PVA$. The absorption peaks corresponding to TiO_2 and $(TBA)_4PW_{11}Fe$ can be clearly seen in the spectra of the prepared nanocomposite. As shown in Fig. 2(b), the spectra of $(TBA)_4PW_{11}Fe@TiO_2@PVA$ consisted of some peaks at 264 nm and in the range of 330-430 nm. The remarkable peak at 264 nm is mainly attributed to the charge-transfer transition (CT) of $O^{2-}\rightarrow W^{6+}$ in $[PW_{11}Fe(H_2O)O_{39}]^{4-}$ heteropolyanions [43]. The

recorded shoulder peaks in the region of 330-360 nm are considered as CT transition of O–Ti. Also, the peaks around 420 nm are due to the *d–d* transition of iron ions in $(TBA)_4PW_{11}Fe@TiO_2@PVA$ compound [44]. The results illustrate the successful composition of materials.

(Fig. 2)

X-ray diffraction patterns of the samples in the range of $10° \leq 2\theta \leq 60°$ are shown in Fig. 3. The small broad peak at the 2θ values of 19.20, 22.94, and 41.12° in the XRD pattern of PVA showed that the polymer is amorphous (Fig. 3(a)) [22]. As shown in Fig. 3(b), the diffraction peaks corresponding to anatase TiO_2 exhibited peaks at 2θ of 25.35, 27.65, 37.95, 48.20, 54.20, 55.25° [35]. The XRD pattern of $(TBA)_4PW_{11}Fe$ revealed intense peaks at the position of 16.13, 19.07, 21.59, 22.79, 23.81, 29.75, 30.65, 31.45, 35.63, and 36.23° (Fig. 3(c)) [27]. These diffraction peaks were matched well with Keggin-type HPOM as indexed with the JCPDS 00-050-0654. On the other hand, we observed the PVA, TiO_2, and $(TBA)_4PW_{11}Fe$ diffraction peaks in the pattern of synthesized nanocomposite (Fig. 3(d)). This indicated that the HPOM clusters were immobilized effectively on the surface of support materials. At the same time, the typical peaks of $(TBA)_4PW_{11}Fe$ and TiO_2 noticeably shifted to low 2θ values after their composition. This suggested that the intermolecular interaction of PVA polymer has been destroyed by introducing metal oxides unites [45]. The average crystallite size of $(TBA)_4PW_{11}Fe@TiO_2@PVA$ was estimated to be about 33.20 nm by means of Debye-Scherrer equation (Eq. 2).

$$A_c = \frac{0.94\lambda}{\beta \cos\theta} \tag{2}$$

where A_c is the average crystallite size (nm), λ is the X-ray wavelength (0.15406 nm), β is full peak width at half max (FWHM) in radians, and θ is the half of the diffraction angle.

(Fig. 3)

Fig. 4 depicts the SEM images illustrating the surface morphology of bulk materials and $(TBA)_4PW_{11}Fe@TiO_2@PVA$ nanocomposite. The surface image of the PVA polymer seems to be a smooth and flat sheet. In the case of TiO_2 and (TBA)PWFe compounds, it can be found that their particles with irregular shapes were agglomerated (Fig. 4(b and c)). The evidence of the immobilization of metal oxides particles on the surface of PVA was given by SEM as shown in Fig. 4(d). It is clear that the surface of the $(TBA)_4PW_{11}Fe@TiO_2@PVA$ nanocomposite is totally different from that of the bulk materials. Also, the spherical particles of metal oxides in nano-sized diameter were well-dispersed on the polymer matrix.

(Fig. 4)

3.2. ODS process results of model oils and real gas oil

In this work, the effect of nature of the thiophenic substrate as a first parameter was carried out over the $(TBA)_4PW_{11}Fe@TiO_2@PVA$ nanocomposite as the catalyst. As mentioned in the experimental section, the different types of model oils were prepared by dissolving BT, DBT, 4-MDBT, and 4,6-DMDBT in *n*-heptane with an initial concentration of 500 ppm for each compound. In all cases, the $(TBA)_4PW_{11}Fe@TiO_2@PVA$ catalyst (0.10 g), H_2O_2/HOAc oxidant (6 mL), and MeCN extraction solvent (10 mL) were used. Also, desulfurization reactions were performed at a temperature of 60 °C and at atmospheric pressure. After 2 h of the ODS process, the results of the study demonstrated that the removal efficiencies (%) of sulfur compounds were decreased in the following order: DBT (99%) > 4,6-DMDBT (98%) > 4-MDBT (97%) > BT (96%). It can be concluded that the desulfurization of the DBT substrate, which can be remarkably difficult to treat, is higher in the presence of $(TBA)_4PW_{11}Fe@TiO_2@PVA$ phase-transfer catalyst. The observed reactivity trend of thiophenic compounds is very similar to those obtained in the literature and it is associated with the partial electron charge on the sulfur atom and some steric hindrance [46]. The trend of electron charge of sulfur atom in those compounds was 4,6-DMDBT(5.760) > 4-MDBT

(5.759) > DBT (5.758) > BT (5.696) [47]. It can be speculated that the reactivity of substrates in ODS increases as the electron density increase. On the other hand, the steric hindrance of two methyl groups in 4,6-DMDBT causes higher removal efficiency in comparison with 4-MDBT [48]. To further elucidate the success of the designed ODS system, the typical real gas oil was treated under the same condition. The data recorded before and after ODS tests are reported in Table 1. It is pointed out that the total sulfur content was obviously reduced from 0.9848 to 0.0297 wt.% with 97% efficiency. Another concept relevant was attributed to the removal of foul-smelling and highly corrosive sulfur species such as mercaptans. The results indicated the obvious reduction of mercaptans level from 287 to 10 ppm. It must be highlighted that the other specifications of gas oil such as density, water content, viscosity, color, and pour point mainly remained unaffected after ODS treatment.

(Table 1)

From a process optimization perspective, the effect of type of acid used on the removal efficiency of sulfur compounds was studied. The initial conditions adopted were 0.10 g of $(TBA)_4PW_{11}Fe@TiO_2@PVA$ catalyst, 6 mL of the mixture of H_2O_2 and different acids (in v/v ratio of 1:1), and 10 mL of MeCN. The data in Table 2 rendered the best ODS results are found using H_2O_2/HOAc oxidant at 60 °C after 2 h. It can be shown that the carboxylic acids can promote ODS efficiency due to the *in situ* generation of peroxyacids or peracids as the most powerful oxidizing agents. Significantly, they are capable to oxidize the thiophenic compounds without forming a considerable amount of residual by-products. In the presence of carbonic acid, the removal efficiencies of BT, DBT, 4-MDBT, 4,6-DMDBT, and the sulfur content of gas oil were very low. Therefore, the mixture of H_2O_2/HOAc was selected as the suitable oxidant for forthcoming ODS reactions.

(Table 2)

A fundamental understanding of the catalytic activity of the synthesized materials is necessary in order to optimize the ODS system. Hence, the behavior of $(TBA)_4PW_{11}Fe$, TiO_2, PVA, and $(TBA)_4PW_{11}Fe@TiO_2@PVA$ phase-transfer catalyst were evaluated in desulfurization reactions. Comparatively, with no catalyst, the removal efficiency of BT, DBT, 4-MDBT, 4,6-DMDBT, and the sulfur content of gas oil was 18, 20, 18, 19, and 17%, respectively. As listed in Table 3, the efficiency of the ODS process using the above materials was ranked as follows: $(TBA)_4PW_{11}Fe@TiO_2@PVA$ > $(TBA)_4PW_{11}Fe$ > TiO_2 > PVA. The results evidently indicated that the immobilization of Keggin-type $(TBA)_4PW_{11}Fe$ clusters on TiO_2@PVA matrix offers an attractive way for the preparation of the highly active catalyst. A possible reason for this may be the nature of the $(TBA)_4PW_{11}Fe@TiO_2@PVA$ due to its phase-transferring properties, which enhances oxidation of organic sulfur compounds. In fact, the lipophilicity of quaternary ammonium chains in $(TBA)_4PW_{11}Fe$ can increase the mass transfer in the interfacial region.

(Table 3)

The influence of $(TBA)_4PW_{11}Fe@TiO_2@PVA$ catalyst dosage was analyzed for the desulfurization of the model oils and real gas oil. Due to the high desulfurization reactivity of DBT compound, it was chosen as a representative substrate in the following ODS runs. As shown in Fig. 5, the desulfurization tests of DBT and the sulfur content of gas oil were conducted using various quantities of catalyst (0.02, 0.04, 0.06, 0.08, and 0.10 g) at 60 °C for 2 h. According to the results obtained, the significant efficiency was observed when the applied catalyst dosage was ≥ 0.08 g. It means the dosage of the catalyst has a high-impact on the ODS process. The removal efficiency of DBT and the sulfur content of gas oil reached 99% and 97% using only 0.10 g of $(TBA)_4PW_{11}Fe@TiO_2@PVA$ catalyst, respectively. Consequently, 0.10 g of catalyst was selected as an optimum dosage.

(Fig. 5)

In Fig. 6, the removal efficiency of DBT and the sulfur content of gas oil at different reaction time (0-120 min) and temperature (30, 40, 50, and 60 °C) were compared. The results demonstrated that, at a constant temperature, the removal efficiency of sulfur compounds greatly increased upon increasing the reaction time. The maximum efficiency was achieved after 2 h. Moreover, the desulfurization rate gradually increased as the reaction temperature increased. Under the same conditions, it was established that the highest ODS efficiency can be achieved from 60% at 30 °C to nearly 98% at 60 °C within 2 h. However, a further increase in the reaction temperature had no effect on the removal efficiencies of sulfur compounds. This could be attributed to the thermal decomposition of H_2O_2 at high temperature [49].

(Fig. 6)

3.3. Proposed mechanism of ODS process

In the present work, the ODS system was composed of a non-polar phase (model oils or gas oil), polar phase (H_2O_2/HOAc), and $(TBA)_4PW_{11}Fe@TiO_2@PVA$ phase-transfer catalyst. The mechanism of sulfur oxidation can be explained as follows. Initially, H_2O_2 reacts with acetic acid to form peracetic acid and water molecules. In order to activate the catalyst, the oxygen can be transferred from peracetic acid to terminal metal-oxygen groups ($W=O_d$) of $[PW_{11}Fe(H_2O)O_{39}]^{4-}$ anion. At this time, the new species which are called oxoperoxo metal,$(WO_2)_n$, are generated in the reaction medium [27,43,50]. The quaternary ammonium cation with long hydrocarbon chain transfers the oxoperoxo metal species into the non-polar phase [16,31]. The $(WO_2)_n$ species interact with the organic sulfur compounds, forming their corresponding sulfoxides and heteropolyanions. Posteriorly, the active $(WO_2)_n$ compounds can be regenerated by the reaction of $W=O_d$ with H_2O_2/HOAc oxidant over the catalyst surface. In the next oxidation step, the sulfoxide molecules are oxidized to sulfones. The reaction products have a higher polarity than their initial form before the oxidation. Hence, MeCN as the polar extraction solvent can be used to easily remove them.

3.4. Kinetic studies of ODS process

The pseudo-first-order kinetic model is the most commonly used to determine the rate constant (k) and to analyze the mechanism of the ODS process. If $[S]_0$ and $[S]_t$ are respectively assumed as the concentration of sulfur compound at t = 0 and t = t, the k can be found as described below:

$$\frac{d[S]}{dt} = -k[S] \tag{3}$$

$$\int_{S_0}^{S_t} \frac{d[S]}{[S]} = -\int_0^t k dt \tag{4}$$

$$\ln\left[\frac{S_t}{S_0}\right] = -kt \Rightarrow \left[\frac{S_t}{S_0}\right] = e^{-kt} \tag{5}$$

The variation of concentration $[S]_t/[S]_0$ of DBT and the sulfur compounds in gas oil with time (t) are shown in Fig. 7. It is obvious that the plots of $[S]_t/[S]_0$ or ln $[S]_t/[S]_0$ versus t gives a straight line, which indicates that the ODS rates of sulfur molecules over $(TBA)_4PW_{11}Fe@TiO_2@PVA$ phase-transfer catalyst can be appropriately described using the pseudo-first-order model. The kinetic parameters obtained at 30, 40, 50, and 60 °C are summarized in Table 4. It can be concluded that the correlation coefficient (R^2) values are found close to unity (~ 1). It is also noted that the k parameter increases with increasing the reaction temperature in the order of 60 °C > 50 °C > 40 °C > 30 °C. In addition, the apparent activation energies (E_a) can be calculated by plotting a graph of ln k versus $1/T$ and obtaining their slopes (Eq. 6 and Fig. 8). The assessed E_a values for the ODS of DBT and sulfur compounds of gas oil were 32.00, and 26.78 kJ/mol, respectively. Based on Fig. 8, the plots showed high values of R^2, which imply that the Arrhenius plot is suitable in order to attain the activation energy of the sulfur oxidation using designed ODS system.

$$k = Ae^{\frac{-E_a}{RT}} \Rightarrow \ln k = \frac{-E_a}{R}\left(\frac{1}{T}\right) + \ln A \tag{6}$$

where E_a is the apparent activation energy; R is the gas constant (8.314 J/mol.K); and T is the reaction temperature (Kelvin), respectively.

(Fig. 7)

(Fig. 8)

(Table 4)

3.5. Reusability of $(TBA)_4PW_{11}Fe@TiO_2$@PVA catalyst

To assess the reusability performance of $(TBA)_4PW_{11}Fe@TiO_2$@PVA in ODS treatments, a set of five successive experiments were carried out under the condition of catalyst = 0.10 g, DBT-containing model oil = 50 mL, H_2O_2/HOAc = 6 mL, MeCN = 10 mL, temperature = 60 °C, and time = 2 h. At the end of each catalytic ODS test, the oil phase was analyzed by XRF and the removal efficiency of DBT was calculated. The results provided in Table 5 shows that the phase-transfer catalyst can be recycled five times. The removal efficiency of DBT compound was dropped slightly from 99 to 94% after five runs. The decrease in the desulfurization efficiency could be attributed to the small mass loss of $(TBA)_4PW_{11}Fe@TiO_2$@PVA catalyst during recycling. The ODS results of real gas oil using the recovered catalyst after the first run are reported in Table 1. It is indicated that the desulfurization results are quite close to the results obtained with fresh catalyst. The results revealed that the $(TBA)_4PW_{11}Fe@TiO_2$@PVA nanocomposite is a promising phase-transfer catalyst in such both terms catalytic activity and reusability for ODS technology of fuel oils.

(Table 5)

4. Conclusions

In conclusion, the $(TBA)_4PW_{11}Fe$ clusters have been prepared and immobilized on TiO_2@PVA support materials by the sol-gel method. The characterization results proved the successful composition of the materials and the fabrication of $(TBA)_4PW_{11}Fe@TiO_2$@PVA

catalyst. The catalytic activity of the composite was evaluated in ODS reactions of model oils and gas oil. The effects of the main process variables were investigated thoroughly. Based on the results, the catalyst showed outstanding performance in deep removal of thiophenic compounds from the oil phase. Notably, the efficiency of DBT removal reached 99% over $(TBA)_4PW_{11}Fe@TiO_2@PVA$ phase-transfer catalyst using H_2O_2/HOAc oxidant. Also, the report indicated that the kinetics of sulfur oxidation process followed the pseudo-first-order model. According to the results of catalyst recycling, it was noted that the recycled use of the catalyst for five times did not conspicuously affect its activity. We believe the synthesis of $(TBA)_4PW_{11}Fe@TiO_2@PVA$ nanocomposite can provide valuable knowledge for the development of highly efficient phase-transfer catalysts for deep ODS process.

References

[1] J. He, P. Wu, Y. Wu, H. Li, W. Jiang, S. Xun, M. Zhang, W. Zhu, H. Li, ACS Sustainable Chem. Eng., 5 (2017) 8930-8938.

[2] H. Ji, J. Sun, P. Wu, B. Dai, Y. Chao, M. Zhang, W. Jiang, W. Zhu, H. Li, J. Mol. Catal. A: Chem., 423 (2016) 207-215.

[3] A. W. Bhutto, R. Abro, S. Gao, T. Abbas, X. Chen, G. Yu, J. Taiwan Inst. Chem. Eng., 62 (2016) 84-97.

[4] D. V. Wagle, H. Zhao, C. A. Deakyne, G. A. Baker, ACS Sustainable Chem. Eng., 6 (2018) 7525-7531.

[5] A. Earvin Sy Choi, S. Roces, N. Dugos, M. W. Wan, Fuel, 180 (2016) 127-136.

[6] Y. Zhang, R. Wang, Diam. Relat. Mater., 73 (2017) 161-168.

[7] J. Kou, C. Lu, W. Sun, L. Zhang, Z. Xu, ACS Sustainable Chem. Eng., 3 (2015) 3053-3061.

[8] M. A. Rezvani, S. Khandan, Appl. Organometal. Chem., e4524 (2018) 1-13.

[9] Y. Nie, C. Li, A. Sun, H. Meng, Z. Wang, Energy Fuels, 20 (2006) 2083-2087.

[10] A. B. Pereiro, A. Rodríguez, Sep. Purif. Technol., 62 (2008) 733-738.

[11] D. Jha, N. M. Mubarak, M. Belal Haider, R. Kumar, M. S. Balathanigaimani, J. N. Sahu, Fuel, 244 (2019) 132-139.

[12] Y. Qin, S. Xun, L. Zhan, Q. Lu, M. He, W. Jiang, H. Li, M. Zhang, W. Zhu, H. Li, New J. Chem., 41 (2017) 569-578.

[13] V.C. Srivastava, RSC Adv., 2 (2012) 759-783.

[14] K. H. Almashjary, M. Khalid, S. Dharaskar, P. Jagadish, R. Walvekar, T. C. S. Manikyam Gupta, Fuel, 234 (2018) 1388-1400.

[15] J. Luo, J. Xiong, Y. Chao, X. Li, H. Li, J. Pang, F. Zhu, W. Zhu, H. Li, J. Taiwan Inst. Chem. Eng., 93 (2018) 245-252.

[16] M. A. Rezvani, M. Alinia Asli, S. Khandan, H. Mousavi, Z. Shokri Aghbolagh, Chem. Eng. J., 312 (2017) 243-251.

[17] D. Yuan, H. Song, H. Song, M. You, B. Wang, F. Li, Y. Hao, Q. Yu, J. Taiwan Inst. Chem. Eng., 76 (2017) 83-88.

[18] D. Julião, A. C. Gomes, M. Pillinger, L. Cunha-Silva, B. de Castro, I. S. Gonçalves, S. S. Balula, Fuel Process. Technol. 131 (2015) 78-86.

[19] M. C. Capel-Sanchez, J. M. Campos-Martin, J. L. G. Fierro, Energy Environ. Sci., 3 (2010) 328-333.

[20] M. A. Rezvani, Z. Shokri Aghbolagh, H. H. Monfared, S. Khandan, J. Ind. Eng. Chem., 52 (2017) 42-50.

[21] D. Huang, Z. Zhai, Y. C. Lu, L. M. Yang, G. S. Luo, Ind. Eng. Chem. Res., 46 (2007) 1447-1451.

[22] M. A. Rezvani, M. Ali Nia Asli, M. Oveisi, R. Babaei, K. Qasemi, S. Khandan, RSC Adv., 6 (2016) 53069-53079.

[23] A. M. Escobar Caicedo, J. A. Rengifo-Herrera, P. Florian, M. N. Blanco, G. P. Romanelli, L. R. Pizzio, J. Mol. Catal. A: Chem., 425 (2016) 266-274.

[24] A. Patel, N. Narkhede, S. Singh, S. Pathan, Catal. Rev., 58 (2016) 337-370.

[25] D. L. Long, R. Tsunashima, L. Cronin, Angew. Chem. Int. Ed., 49 (2010) 1736-1758.

[26] E. Rafiee, S. Rezaei, J. Taiwan Inst. Chem. Eng., 61 (2016) 174-180.

[27] M. A. Rezvani, S. Khandan, N. Sabahi, Energy Fuels, 31 (2017) 5472-5481.

[28] S. S. Wang, G. Y. Yang, Chem. Rev., 115 (2015) 4893-4962.

[29] W. Zhao, C. Yang, K. Liu, Y. Yang, T. Chang, New J. Chem., 41 (2017) 447-451.

[30] M. A. Rezvani, S. Khandan, M. Aghmasheh, Taiwan. Inst. Chem. Eng. J., 77 (2017) 321-328.

[31] F. Mirante, L. Dias, M. Silva, S. O. Ribeiro, M. C. Corvo, B. Castro, C. M. Granadeiro, S. S. Balula, Catal. Commun., 104 (2018) 1-8.

[32] M. A. Rezvani, O. Feghhe Miri, Chem. Eng. J., 369 (2019) 775-783.

[33] W. Jiang, H. Jia, Z. Zheng, L. Zhu, L. Dong, W. Liu, W. Zhu, H. Li, Pet. Sci. 15 (2018) 841-848.

[34] X. Huang, R. Wang, T. Jiao, G. Zou, F. Zhan, J. Yin, L. Zhang, J. Zhou, Q. Peng, ACS Omega, 4 (2019) 1897-1906.

[35] H. Zhu, R. Jiang, Y. Fu, Y. Guan, J. Yao, L. Xiao, G. Zeng, Desalination, 286 (2012) 41-48.

[36] M. A. Rezvani, M. Shaterian, F. Akbarzadeh, S. Khandan, Chem. Eng. J., 333 (2018) 537-544.

[37] F. Emanuela, C. Claudia, C. A. Lina, P. Patrizia, C. Francesca, C. G. Anna, G. Giuseppe, C. Giuseppe, Appl. Surf. Sci., 331 (2015) 292-298.

[38] M. Ren, F. H. Frimmel, G. Abbt-Braun, J. Mol. Catal. A: Chem., 400 (2015) 42-48.

[39] Y. Haldorai, J. J. Shim, Polym. Composites, 35 (2014) 327-333.

[40] P. Shringarpure, K. Patel, A. Patel, J. Clust. Sci., 22 (2011) 587-601.

[41] K. K. Dey, P. Kumar, R. R. Yadav, A. Dhara, A. Kumar Srivastava, RSC Adv., 4 (2014) 10123-10132.

[42] V. Kaler, U. Pandel, R. K. Duchaniya, Mater. Today: Proc., 5 (2018) 6279-6287.

[43] X. Jiang, H. Li, W. Zhu, L. He, H. Shu, J. Lu, Fuel, 88 (2009) 431-436.

[44] Y. G. Chen, J. F. Liu, Polyhedron, 15 (1996) 3433-3436.

[45] Y. Wang, Z. Wang, P. Ma, H. Bai, W. Dong, Y. Xie, M. Chen, RSC Adv., 5 (2015) 72691-72698.

[46] J. Xiao, L. Wu, Y. Wu, B. Liu, L. Dai, Z. Li, Q. Xia, H. Xi, Appl. Energy, 113 (2014) 78-85.

[47] H. Lü, C. Deng, W. Ren, X. Yang, Fuel Process. Technol., 119 (2014) 87-91.

[48] S. Ribeiro, A. D. S. Barbosa, A. C. Gomes, M. Pillinger, I. S. Gonçalves, L. Cunha-Silva, S. S. Balula, Fuel Process. Technol., 116 (2013) 350-357.

[49] X. Yu, P. Han, Y. Li, RSC Adv., 8 (2018) 17938-17943.

[50] W. S. Zhu, H. M. Li, X. Y. He, Q. Zhang, H. M. Shu, Y. S. Yan, Catal. Commun., 9 (2008) 551-555.

Figures and tables caption

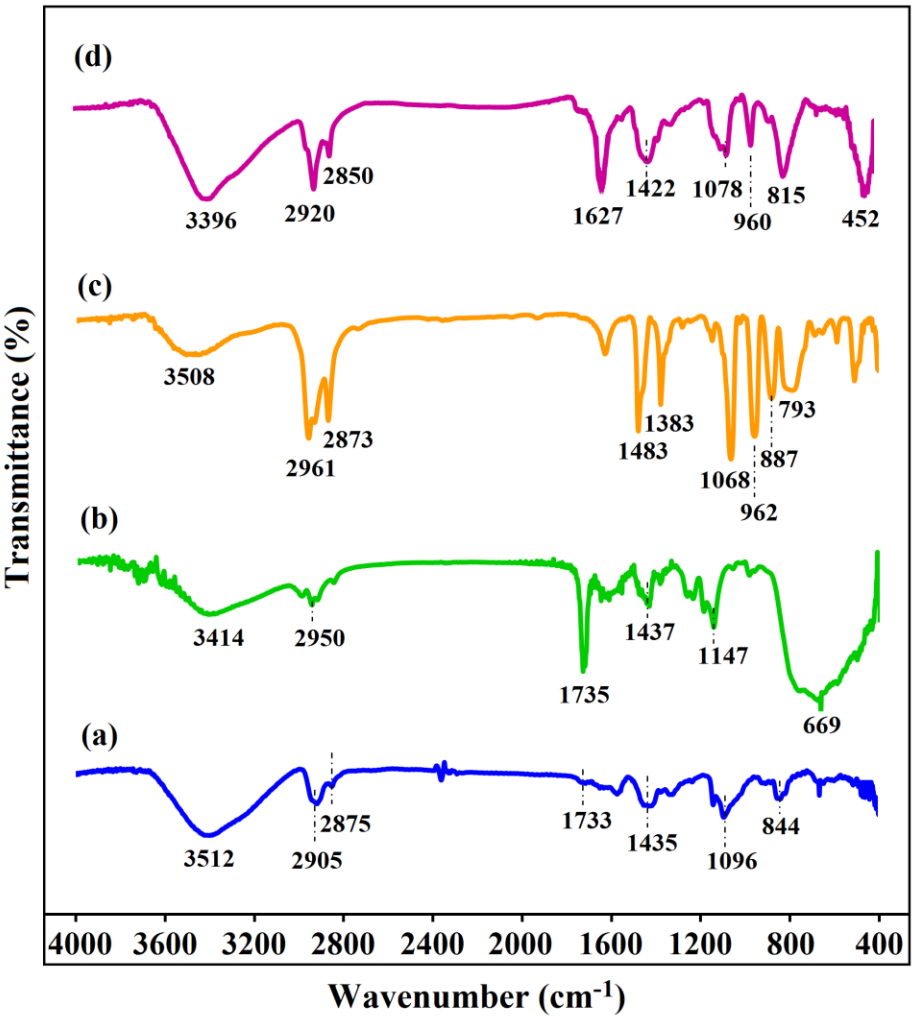

Fig. 1. FT-IR spectra of (a) PVA, (b) TiO_2, (c) $(TBA)_4PW_{11}Fe$, and (d) $(TBA)_4PW_{11}Fe@TiO_2@PVA$ nanocomposite.

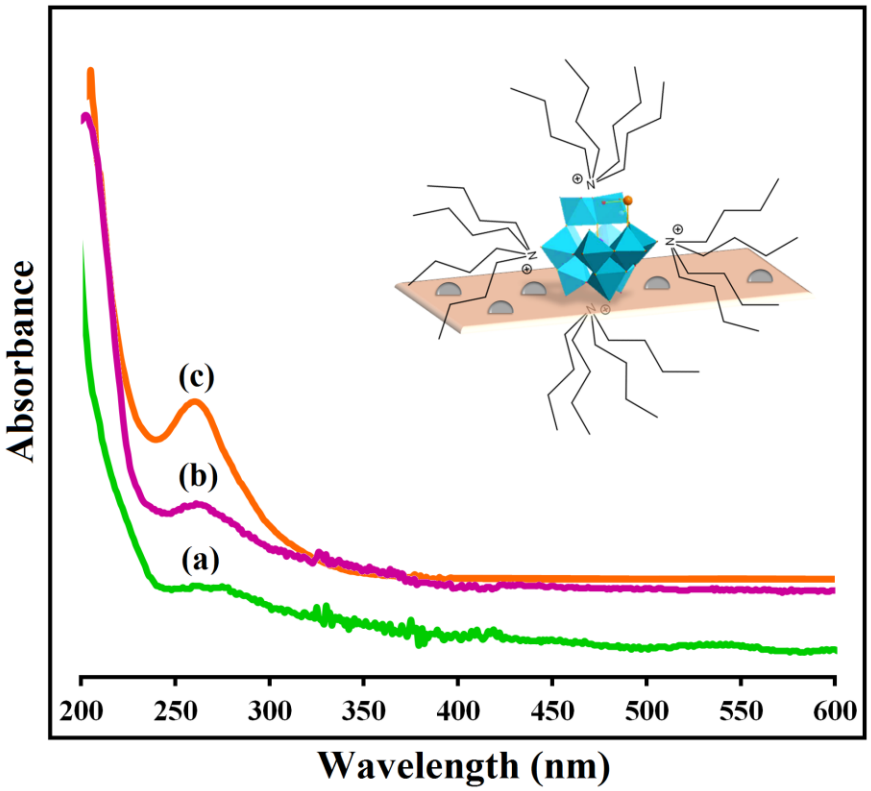

Fig. 2. UV-vis spectra of (a) TiO_2, (b) $(TBA)_4PW_{11}Fe@TiO_2@PVA$ nanocomposite, and (c) $(TBA)_4PW_{11}Fe$.

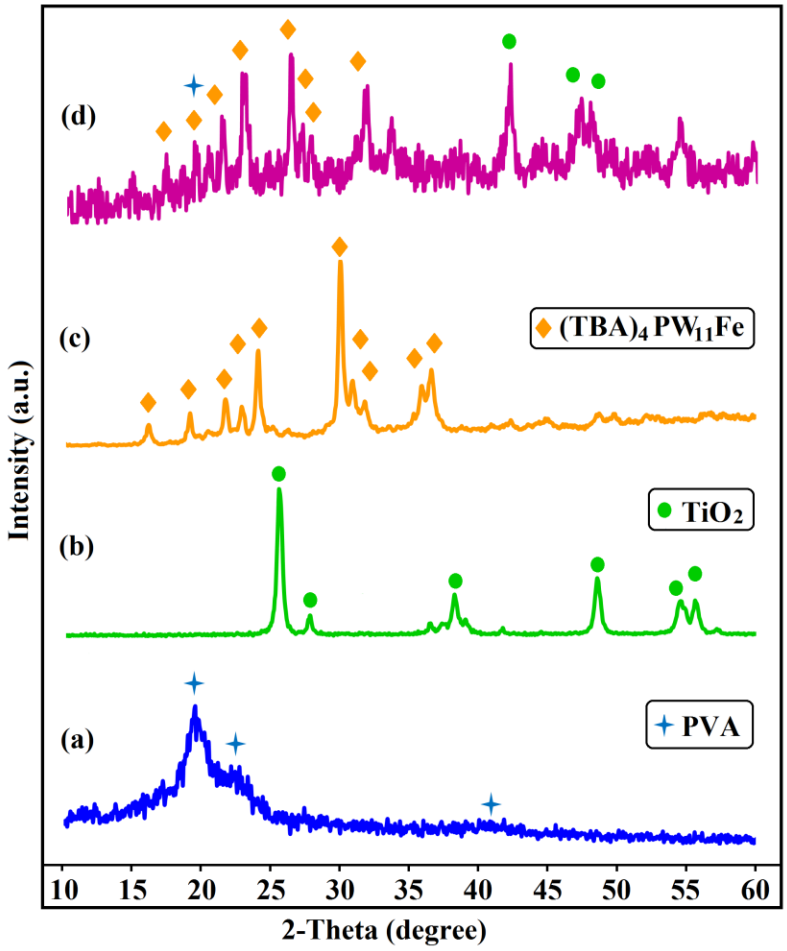

Fig. 3. XRD patterns of (a) PVA, (b) TiO_2, (c) $(TBA)_4PW_{11}Fe$, and (d) $(TBA)_4PW_{11}Fe@TiO_2@PVA$ nanocomposite.

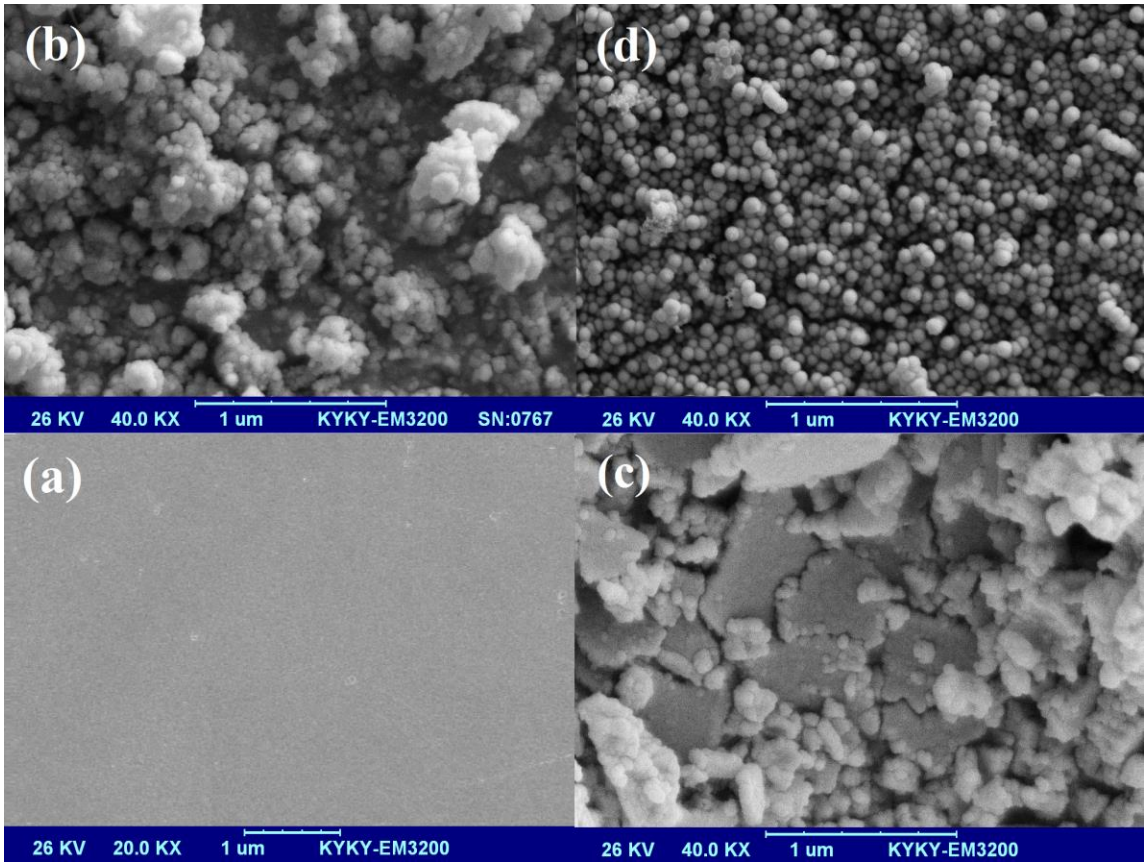

Fig. 4. SEM images of (a) PVA, (b) TiO_2, (c) $(TBA)_4PW_{11}Fe$, and (d) $(TBA)_4PW_{11}Fe@TiO_2@PVA$ nanocomposite.

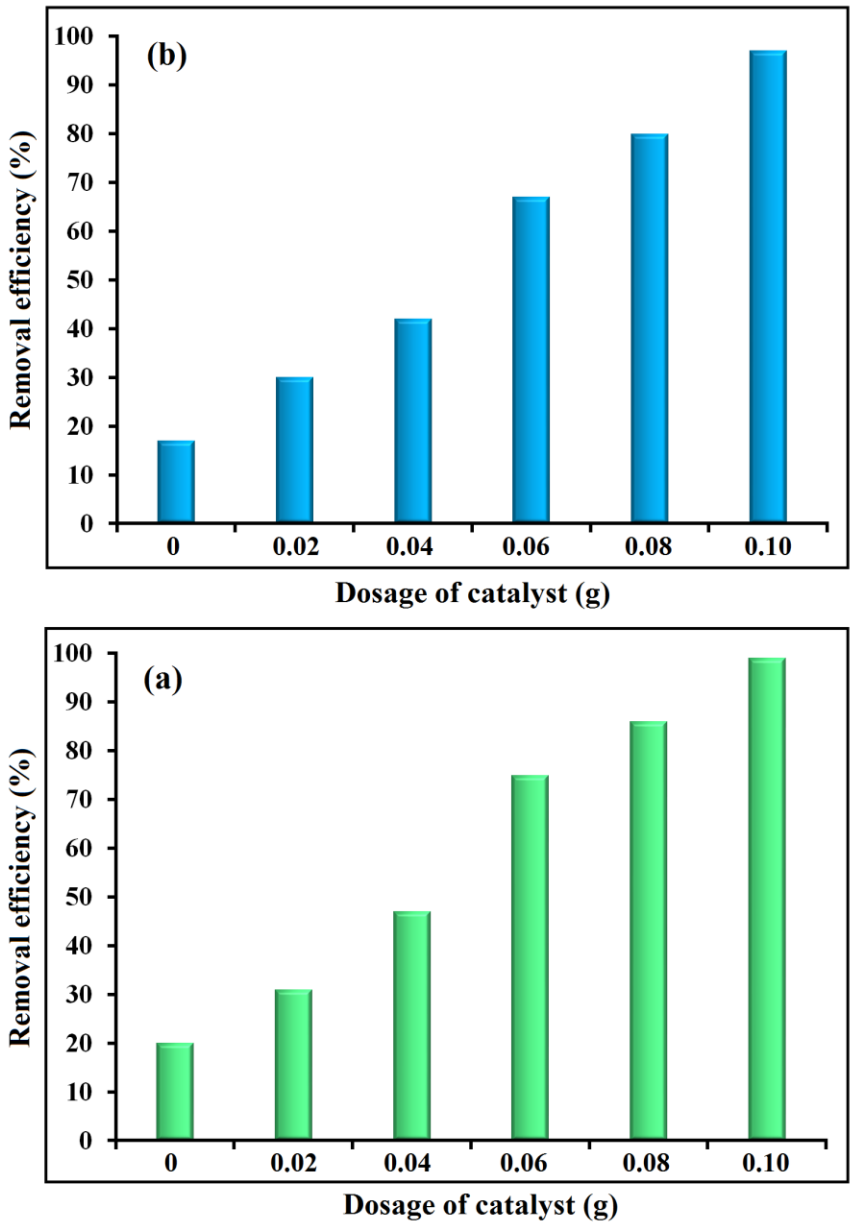

Fig. 5. Effect of $(TBA)_4PW_{11}Fe@TiO_2@PVA$ catalyst dosage on the ODS process of (a) DBT and (b) sulfur content of gas oil.

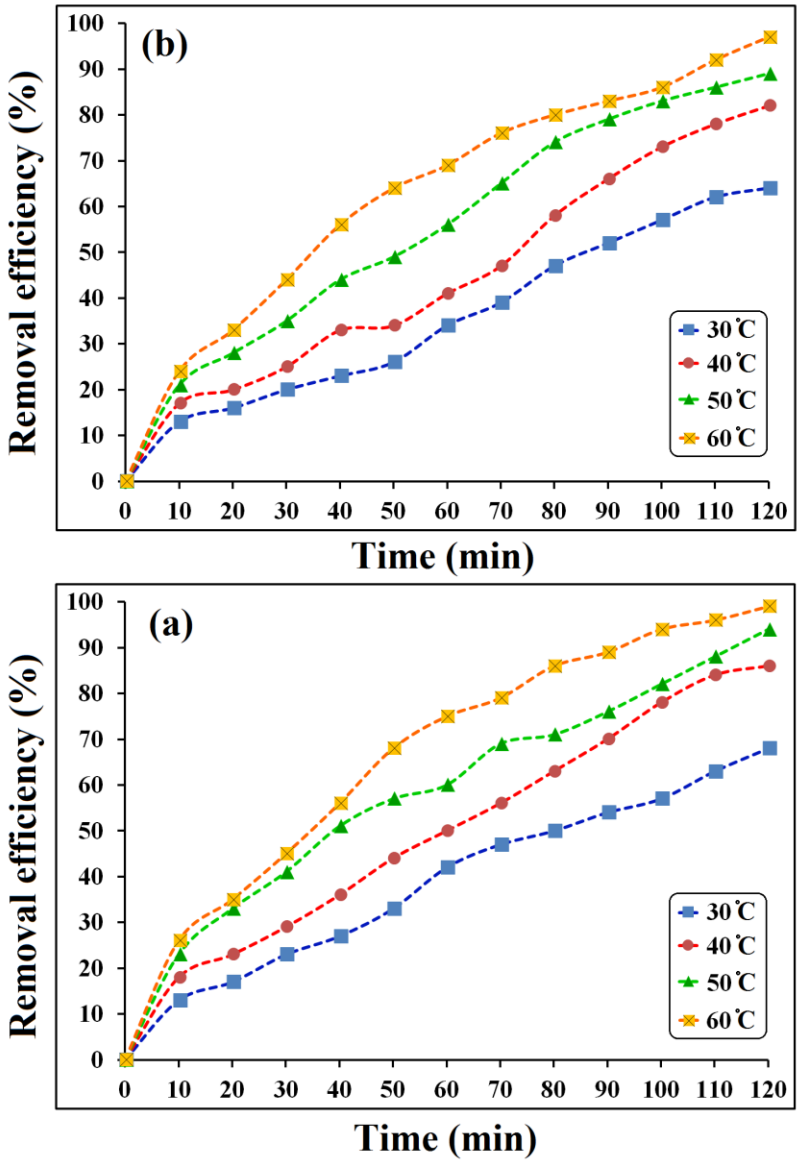

Fig. 6. Effect of reaction temperature and reaction time on the ODS process of (a) DBT and (b) sulfur content of gas oil.

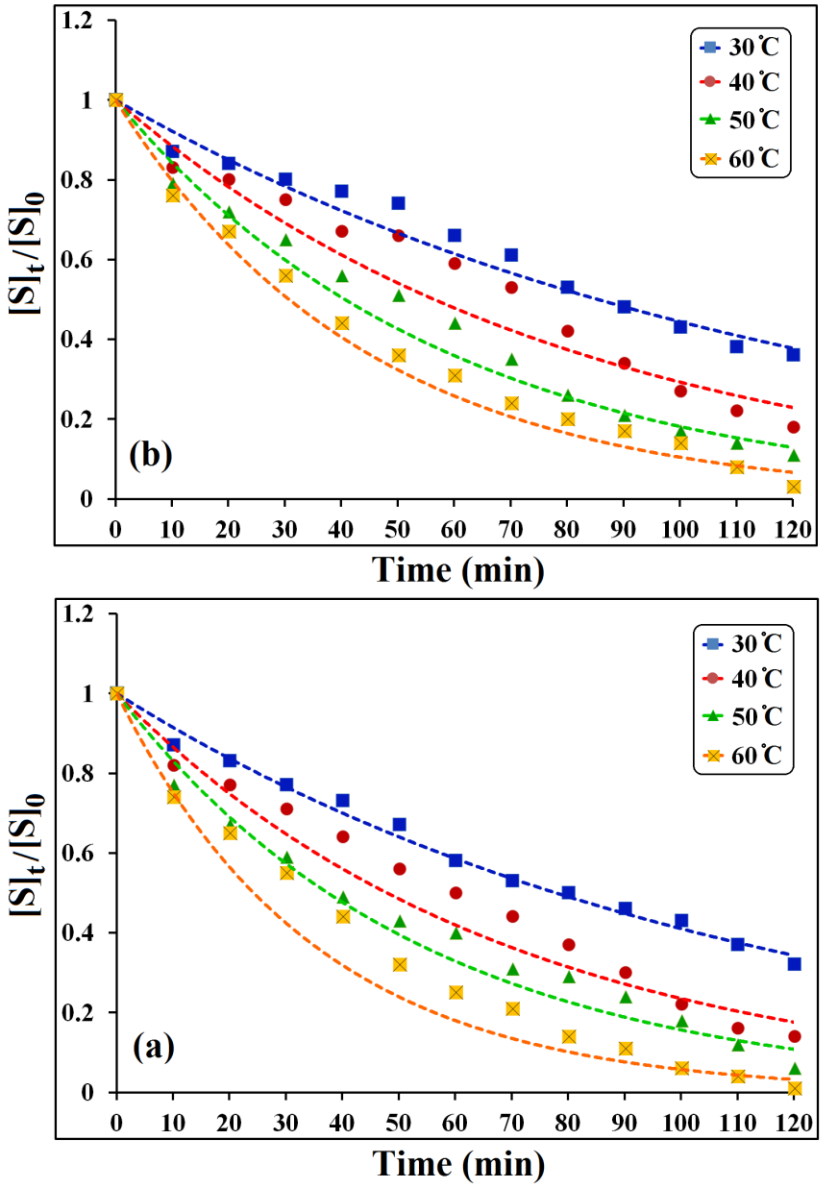

Fig. 7. Plots of $[S]_t/[S]_0$ against time (min) for the ODS process of (a) DBT and (b) sulfur content of gas oil.

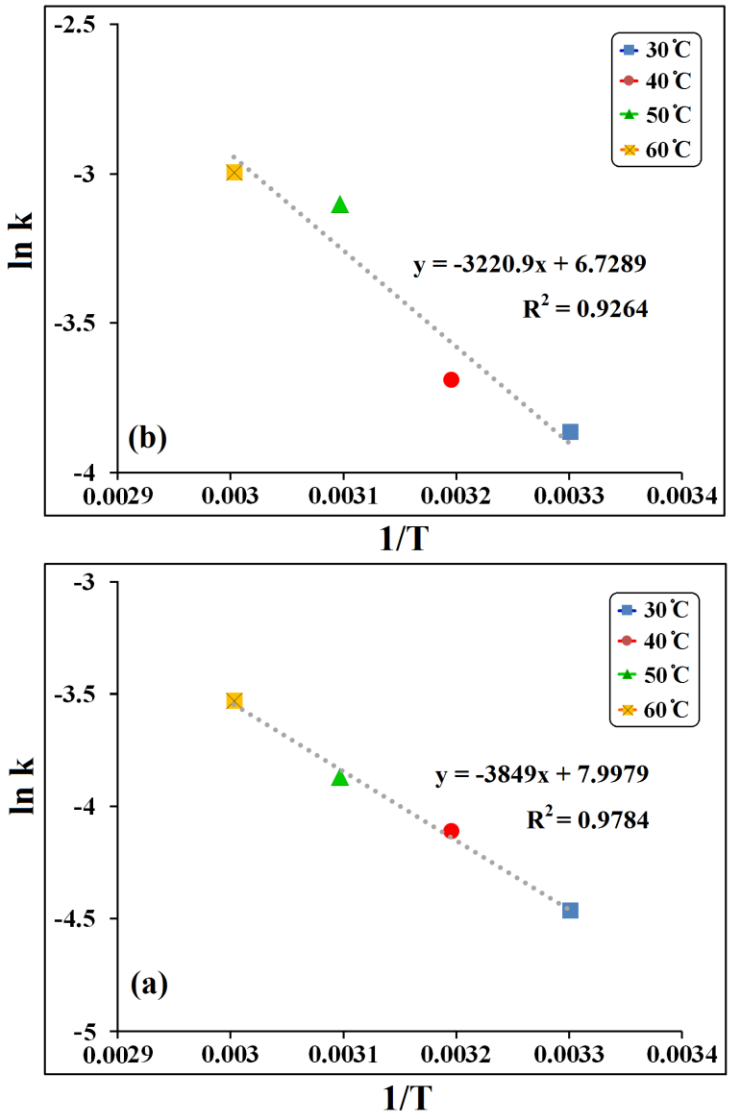

Fig. 8. Plots of ln *k* against 1/*T* for the ODS process of (a) DBT and (b) sulfur content of gas oil.

Table 1. ODS results of real gas oil by $(TBA)_4PW_{11}Fe@TiO_2@PVA$ phase-transfer catalyst.

Table 1. ODS results of real gas oil by $(TBA)_4PW_{11}Fe@TiO_2@PVA$ phase-transfer catalyst.

Entry	Properties of gas oil	Before ODS	After ODS [a]	After ODS [b]
1	Total sulfur content wt. %	0.9848	0.0297	0.0295
2	Density @ 15 °C	0.8366	0.8365	0.8364
3	Mercaptans ppm	287	10	9
4	Flash point (°F)	145	144	144
5	Water content vol. %	0.025	0.025	0.025
6	Cloud point (°C)	-4	-4	-4
7	Color test	1.5	1.5	1.5
8	Viscosity KIN @ 50 °C. CST.	2.9	2.8	2.8
9	Pour point (°C)	-9	-9	-9
10	Distillation (IBP °C)	157.4	157.2	157.1
11	Distillation (FBP °C)	386.6	386.4	386.2

[a] Condition of ODS reaction: 50 mL of gas oil, 0.10 g of catalyst, 6 mL H_2O_2/HOAc, 10 mL of MeCN, time = 2 h, and temperature = 60 °C.
[b] ODS results using reused catalyst.

Table 2. Effect of different acids on the ODS of model oils and real gas oil.

Table 2. Effect of different acids on the ODS of model oils and real gas oil.[a]

Entry	Acid	ODS efficiency (%)				
		BT	DBT	4-MDBT	4,6-DMDBT	Gas oil
1	Acetic acid	96	99	97	98	97
2	Benzoic acid	88	91	89	89	89
3	Oxalic acid	88	90	89	88	88
4	Sulfuric acid	71	75	72	73	72
5	Carbonic acid	70	73	71	71	70

[a] Condition of ODS reaction: 50 mL of gas oil or model oil, 0.10 g of catalyst, 3 mL of H_2O_2, 3 mL of acid, 10 mL of MeCN, time = 2 h, and temperature = 60 °C.

Table 3. Effect of different catalysts on the ODS of model oils and real gas oil.

Table 3. Effect of different catalysts on the ODS of model oils and real gas oil.[a]

Entry	Catalyst	ODS efficiency (%)				
		BT	DBT	4-MDBT	4,6-DMDBT	Gas oil
1	$(TBA)_4PW_{11}Fe@TiO_2@PVA$	96	99	97	98	97
2	$(TBA)_4PW_{11}Fe$	68	69	70	72	68
3	TiO_2	52	55	53	54	51
4	PVA	20	23	25	26	24
5	None	18	20	18	19	17

[a] Condition of ODS reaction: 50 mL of gas oil or model oil, 0.10 g of catalyst, 6 mL of H_2O_2/HOAc, 10 mL of MeCN, time = 2 h, and temperature = 60 °C.

Table 4. Pseudo-first-order rate constants and correlation factors of DBT in model oil and sulfur compounds in real gas oil at different temperatures.

Table 4. Pseudo-first-order rate constants and correlation factors of DBT in model oil and sulfur compounds in real gas oil at different temperatures.

Temperature (°C)	Rate constant (k)		Correlation factor (R^2)	
	DBT	Sulfur compounds	DBT	Sulfur compounds
30	0.009	0.008	0.9898	0.9712
40	0.014	0.013	0.9440	0.9281
50	0.019	0.017	0.9249	0.9747
60	0.029	0.023	0.8957	0.9204

Table 5. Reusability of $(TBA)_4PW_{11}Fe@TiO_2@PVA$ phase-transfer catalyst for ODS of DBT compound.

Table 5. Reusability of $(TBA)_4PW_{11}Fe@TiO_2@PVA$ phase-transfer catalyst for ODS of DBT compound.[a]

Run	ODS efficiency (%)
1	99
2	98
3	96
4	95
5	94

[a] Condition of ODS reaction: 50 mL of model oil, 0.10 g of catalyst, 6 mL of H_2O_2/HOAc, 10 mL of MeCN, time = 2 h, and temperature = 60 °C.